Fully Automated On-Wafer Noise Characterization of GaAs MESFET's and HEMT's

John W. Archer, *Fellow, IEEE*, and Robert A. Batchelor

***Abstract*—A technique is described which enables the rapid determination of all four noise parameters of a MESFET or HEMT at wafer level. The fully automated procedure, which has been implemented in the 2–18 GHz range, uses 16 accurately measured, very repeatable source impedance standards. The standards have been selected for optimum coverage of the input impedance plane to result in stable and rapidly convergent least-squares solutions for the minimum noise figure, optimum source impedance and noise resistance of practical devices. The resultant system is very stable and produces accurate noise parameters for a wide range of devices.**

I. Introduction

THE USE of on-wafer microwave probing systems enables evaluation of the performance of microwave devices and MMIC's without the need for dicing and mounting of individual chips in microwave packages. This means that only chips meeting performance specifications need be mounted, resulting in improved production efficiency. Microwave probers also provide a valuable aid in determining device parameters, free of package parasitics, for the design of MMIC's.

While the major use of on-wafer probing was initially for measuring S-parameters in association with automatic network analyzers [1], the technique is also used for obtaining noise performance [2], and several packages are available that enable full noise characterization of devices on wafer [3], [4].

In this paper we describe an automatic system for determining a set of four noise parameters of FET's and HEMT's. Use of an electronic means of varying source impedance, and careful consideration of possible sources of error, result in a system which gives accurate and repeatable results. The system operates over the band 2–18 GHz and is capable of measuring noise figures down to a few tenths of a dB with an accuracy of ± 0.2 dB rms. A range of source impedances is presented to the device under test (DUT) and the noise parameters are derived using a least-squares fitting procedure. The system is capable of good accuracy and throughput. Simple changes would enable measurement of low-noise MMIC's. Although the application for which the system has been developed is on-wafer probing, the basic method can be applied to coaxial or similar environments, and would facilitate measurement of cooled devices.

Manuscript received April 2, 1991; revised September 17, 1991.

The authors are with the Solid-State Devices Group of the CSIRO Division of Radiophysics, Vimiera and Pembroke Roads, Marsfield, NSW 2121, Australia.

IEEE Log Number 9104784.

II. Noise Measurement

Four parameters are required to characterize fully the noise performance of a linear two-port network [5]. There is a variety of parameter sets that can be used and any set can be transformed into another [6]. The parameter set used in this work consists of the minimum noise figure ($F_{\min}$), the complex source reflection coefficient at which the minimum occurs (Γ_{opt}), and the noise resistance (r_n), a parameter which measures the rate of increase of noise figure as the source impedance departs from optimum. These noise parameters can be determined by presenting a range of source impedances to the DUT and measuring the noise figure corresponding to each impedance. A computer analysis is then used to determine the noise parameters [7]. The noise figure (F) corresponding to any source reflection coefficient (Γ_s) can be expressed as follows:

$$F = F_{\min} + \frac{4r_n}{Z_0} \frac{|\Gamma_{opt} - \Gamma_s|^2}{|1 + \Gamma_{opt}|^2(1 - |\Gamma_s|^2)} \quad (1)$$

where Z_0 is the characteristic impedance of the measuring system, usually 50 Ω [8].

The usual method of measuring noise figure is to determine the output change corresponding to a known increment in the input noise. Today this is often accomplished using a switched noise source at the DUT input and an automatic noise figure meter at the output port. To obtain a noise parameter set, a means of presenting a range of source impedances to the DUT is required. This is usually accomplished by inserting a tuner between the noise source and the DUT. At each setting of the tuner the impedance presented to the device and the tuner insertion loss must be known. There are a number of variations on this technique. In the "noise wave method" a sliding short circuit is used [8], [9]. Another variation uses a programmable attenuator and a short circuit to provide the impedance change [10]. A long line, coupled with a small frequency change has been used to increase impedance coverage [10]. Electronic means of changing impedance have been employed [10].

If the DUT is poorly matched at its output port, allowance has to be made for noise incident on the output port being reflected back to the noise figure meter. This is es-

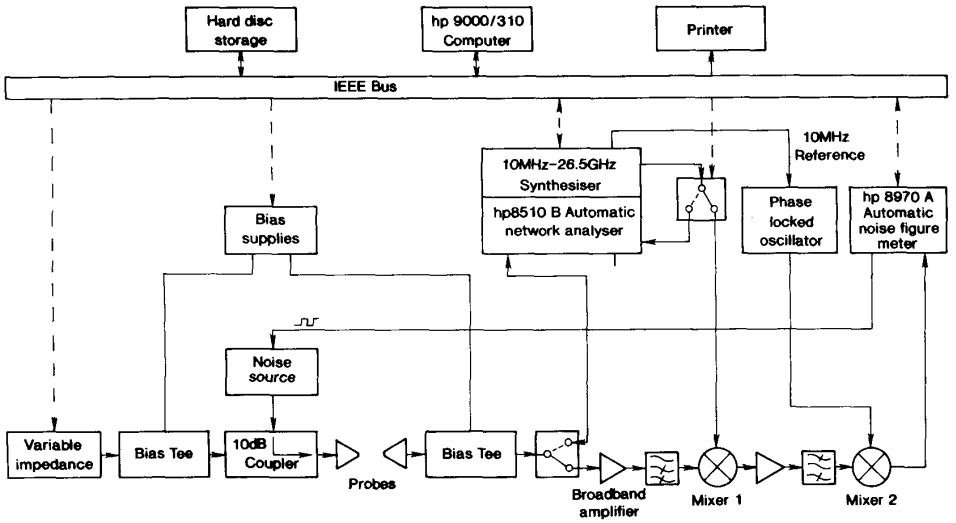

Fig. 1. Block diagram of the on-wafer noise measuring system.

pecially important when measuring FET's and HEMT's, which can have high output reflection coefficient. An output tuner can be used to provide a match between the DUT and the noise figure meter, making due allowance for its insertion loss. This requires an adjustment for each input impedance presented and hence is not very efficient. A better method is to measure the output reflection coefficient for each source impedance and apply a correction.

III. On-Wafer Noise Measurement

The block diagram of Fig. 1 illustrates the measurement system that is the subject of this paper. A switched noise source (hp346C) is coupled to the device input via a 10 dB directional coupler. Source impedance variation is obtained by varying the dc bias applied to a p-i-n diode switch. This provides radial coverage of the Smith chart. Circumferential coverage is obtained by varying the frequency. Because of the long line between the p-i-n diode and the DUT a small change of frequency results in a large impedance variation. For the typical range of frequency used (e.g., 4720 to 4795 MHz, 1.6 percent) the noise parameters of most devices can be assumed to be constant. Fig. 2 shows, plotted on a Smith chart, the impedances presented to a DUT for frequencies between 4720 and 4795 MHz. Similar plots are obtained at other frequencies in the operating band of the instrument. Radial coverage of the Smith chart is restricted to magnitudes of reflection coefficient less than about 0.6 by the losses associated with the probe, 10 dB coupler, input line and bias T. Use of an electronic means of impedance variation assures repeatability, and avoids the problem of remotely driving a mechanical tuner with its associated vibration, which could be a problem with delicate probe contacts.

The DUT output is connected, via a bias T and switch, to a receiver which employs a double frequency conversion system. A low-noise, broadband pre-amplifier is followed by a mixer and a high-pass filter which then couple to a 4.78 GHz pre-amplifier, a bandpass filter and a second mixer. The local oscillator for the first mixer is derived from the synthesized frequency source of a hp8510B automatic network analyzer, while the second mixer is fed by an oscillator phase locked to the hp8510B's low frequency reference oscillator. The output from the receiver is connected to a hp8970A automatic noise figure meter. The output probe can be switched to either the noise measurement receiver or the hp8510B network analyzer. A hp9000/310 computer controls the switching, p-i-n diode bias and frequency changing together with data collection and processing. It is also used to control the hp8510B automatic network analyzer during input calibration and measurement of the output reflection coefficient.

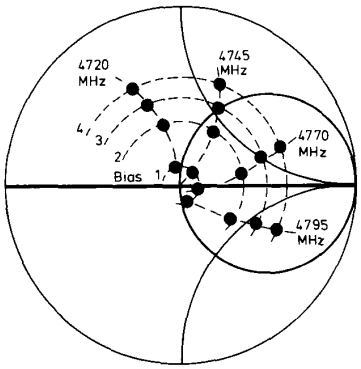

Fig. 2. Impedance plane (Smith chart) representation of a set of input impedances presented to the DUT.

An earlier, narrow band version of this measurement system was centered at 4.78 GHz and was used to develop the concept. In that system the DUT output reflection coefficient was measured using a total power reflectometer. In the current system this measurement is made with the net-

work analyzer. A further refinement to be implemented in the near future will enable, with a single probing operation, the measurement of noise parameters at a selection of frequencies, and S-parameters over the range of the network analyzer.

IV. Calibration

A. Input Calibration

Fig. 3 shows the block diagram of the configurations used for input calibration, which consists of determining the loss between the noise source and the DUT, together with the source reflection coefficients. An automatic network analyzer is connected to the output probe and a 1-port calibration performed at the probe tips using the on-wafer reflection standards provided with the probe station. The probes are then connected to the through-line standard, enabling reflection measurements to be made at the probe tips. A short circuit, open circuit and 50 Ω termination are connected in turn to the side arm of the coupler in place of the noise source, and the reflection coefficients measured at each of the four frequencies and p-i-n diode bias settings. From these results, 16 sets of S-parameters are determined (see Appendix I) and used to obtain the insertion loss between the noise source and DUT. The noise source is connected to the coupled arm and the 16 reflection coefficients representing the source impedances presented to the DUT are measured. This full sequence of measurements is carried out automatically, with manual changing of impedance standards. The calibration data are stored in a file for use by the noise measurement program. Input calibrations remain valid for months.

B. Noise Measurement

At the beginning of a measurement session, the noise source is connected to the broadband preamplifier and the hp8970A noise figure meter is calibrated. After the calibration has been completed, a device is probed and biased via the two bias tees. The reading sequence is then started. The output probe is switched to the network analyzer and for each frequency and p-i-n diode bias, the output reflection coefficient is measured. The output probe is then switched to the broadband pre-amplifier and the noise figure and gain are measured at each bias and frequency. This completes the data taking.

The data for each measurement point are then corrected to remove the effects of the input and output circuits, including allowance for the loss of the output probe, and give the noise figure and associated gain. The device noise temperature (T_{DUT}) corrected for all sources of loss and output reflection coefficient is given by

$$T_{\mathrm{DUT}} = L_i T_M - (1 - L_i) T_a - \frac{(1 - L_p + L_p|\Gamma_0|^2) L_i T_a}{G_M} \tag{2}$$

while the associated gain (G_{as}) is

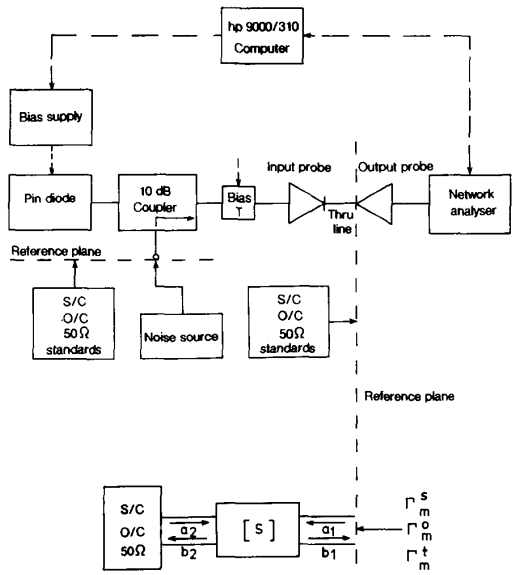

Fig. 3. Block diagram of the input calibration configuration.

$$G_{\mathrm{as}} = \frac{G_M}{L_i L_p (1 - |\Gamma_0|^2)}; \tag{3}$$

L_i the input loss,
T_M the measured noise temperature,
T_a the ambient temperature,
L_p the output probe loss,
G_M the measured gain,
Γ_0 the output reflection coefficient.

The derivation of these equations is given in Appendix II.

Using the corrected noise figures, the program then performs an optimal fit to the data to determine the four noise parameters. The procedure uses a modified Davidon algorithm [11], [12] with a numerically derived Jacobian to minimize an objective function (F_{obj}) which consists of the sum of three terms. The first term is the mean of a weighted difference between the fitted and measured noise figures:

$$F_{\mathrm{obj}} = \frac{1}{N}\left(\sum_{i=1}^{N}\left(1 - \left(\frac{F_{\mathrm{est}}(i)}{F_m(i)}\right)^2\right)^2\left(\frac{\min\,[F_m(i)]}{F_m(i)}\right)^2\right) + \exp\,(-100(1 - |\Gamma_{\mathrm{opt}}|^2)) + \exp\,(250(1 - F_{\mathrm{min}})) \tag{4}$$

where N is the number of data points; and

$$F_{\mathrm{est}}(i) = F_{\mathrm{min}} + \frac{4r_n}{Z_0} \frac{|\Gamma_{\mathrm{opt}} - \Gamma_s(i)|^2}{|1 - \Gamma_{\mathrm{opt}}|^2 (1 - |\Gamma_s(i)|^2)} \tag{5}$$

is the current estimate of F for the ith data point, $F_m(i)$ is the measured noise figure at the ith data point and min $[F_m(i)]$ is the minimum measured noise figure.

The second and third terms are constraints that impose smoothly the conditions, $|\Gamma_{\mathrm{opt}}| < 1$ and $F_{\mathrm{min}} > 1$, respectively. Abrupt imposition of these constraints (i.e.,

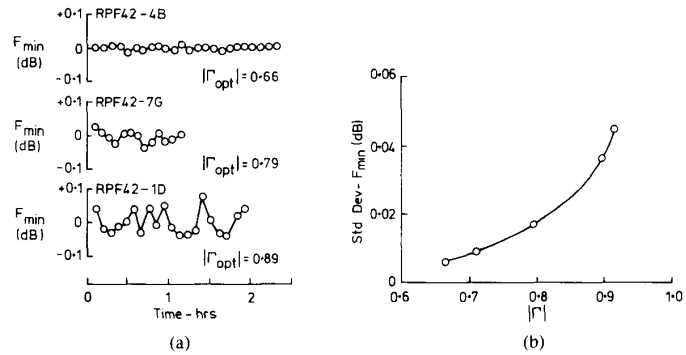

Fig. 4. (a) Results of repeated measurements on devices selected to cover a range of reflection coefficients. (b) Plot of standard deviations of repeated measurements of devices (a) against magnitude of reflection coefficients.

step functions at $|\Gamma_{opt}| = 1$ and $F_{min} = 1$) was found to introduce convergence problems with the fitting algorithm. The scaling coefficients were determined by trial and error and take into account the maximum number magnitude of the computer.

When the minimization process has been completed, the noise parameters are printed out, together with the final value of the objective function. A table containing the measured noise figures, the value of the fitted noise figure at each point, gains and other data, is also produced along with noise figure contours on a Smith chart.

The entire procedure is computer controlled. Device identification and bias conditions are requested, and then the measurements and fitting are carried out without further operator intervention.

V. Results

Routine measurements over a period of several years have shown the system to be convenient to use and very stable. In its current application, evaluating experimental quantities of FET's and HEMT's, its throughput is adequate and could be increased considerably for production purposes by reducing the integration time at each point and reducing the amount of output, most of which has been used to evaluate the measurement system.

Over an interval of 245 days, one device has been measured on 15 occasions at 4.78 GHz. The noise figure of this sample showed an rms scatter about the mean of 0.032 dB, with a spread of 0.093 dB between the maximum and minimum measured noise figures. The noise figure for this device, and others of the same type (NEC NE71000) was 0.45 dB. The data sheet for this device quotes the noise figure to be typically 0.6 dB at 4.0 GHz, while the same device in a package is available in two options with 0.6 dB or 0.45 dB typical noise figure.

Hundreds of experimental devices have now been measured with this system. These devices, depending on geometry, cover a range of noise figures from ~ 0.45 dB to ~ 1.5 dB (at 4.78 GHz). Fig. 4(a) shows the results of repeated measurements on a number of devices, chosen to cover a range of $|\Gamma_{opt}|$. The measurement periods range from about one to two and a half hours. It can be seen that the repeatability is a function of $|\Gamma_{opt}|$, a consequence of the lack of data at high Γ_s. The plot of standard deviation of the measured noise figure as a function of $|\Gamma_{opt}|$ in Fig. 4(b) shows this dependence. The standard deviation in the worst case is a little over 0.04 dB. Twenty-two devices have been measured on different occasions with intervals between measurements ranging from one day to 57 days. The maximum magnitude of the differences between repeated measurements is 0.15 dB while the mean difference is 0.047 dB, indicating that the long-term stability is comparable with the short term. (Both the long- and short-term stability are well within the absolute accuracy of the system.)

The stability of the input calibration at 4.78 GHz was checked several times during a 15-day test period before beginning routine measurements. It was found that the input loss (which is ~ 10 dB) was repeatable to 0.01 dB. (For calibrations taken 15 days apart, the mean of the differences for the 16 source impedances was 0.01 dB.) For the same tests, $|\Gamma|$ was constant to within 0.002 and the phase of Γ changed by about 1° (most of which was due to slightly different probe separations for different calibrations). Another set of input calibrations, covering a period of 112 days, and using a different input probe, resulted in an rms error in the input loss of 0.035 dB. Tests in which the p-i-n diode temperature was varied over a 9 K range showed that the measured noise figure changed by ~ 0.04 dB per 1 K change of p-i-n diode temperature.

The diagram of Fig. 5(a) shows the final value of the objective function (which is a measure of the quality of the fit to the data, with smaller numbers indicating a better fit) plotted against $|\Gamma_{opt}|$, for a large sample of results. The solid curve shows the limits placed on the value of the objective function by the constraints employed. The example given is for a device with a minimum noise figure of 0.2 dB. (The effect on the boundary of increasing the noise figure is indicated by the arrow in the diagram.) Fig. 5(b) is a plot of the relationship between the final value of the objective function and the mean deviation of the fitted noise figures from the measurements. The poor-

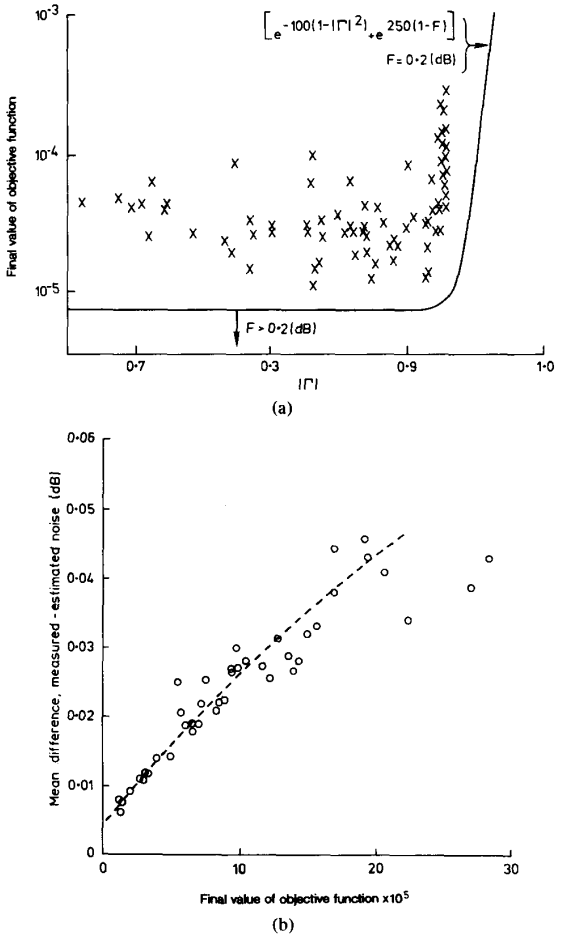

Fig. 5. (a) Plot of the magnitude of the reflection coefficient versus the final value of the objective function for a sample of measured data points. (b) Plot of the final value of the objective function versus mean deviation from the best fit curve for measured data points.

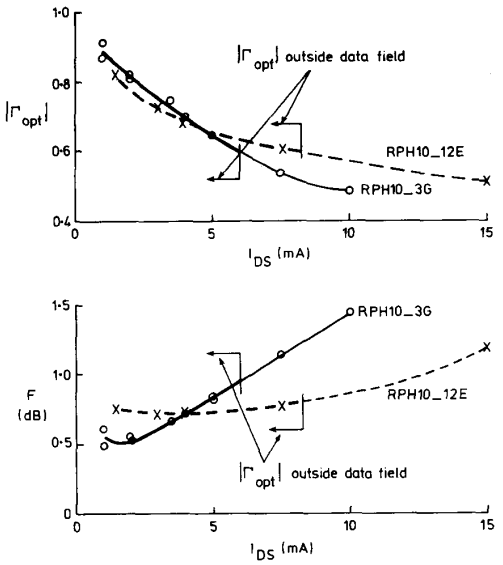

Fig. 6. Plots of noise figure and $|\Gamma_{opt}|$ against drain-source current for two HEMT's, showing smooth behavior as $|\Gamma_{opt}|$ varies from within the field of data points to well outside it.

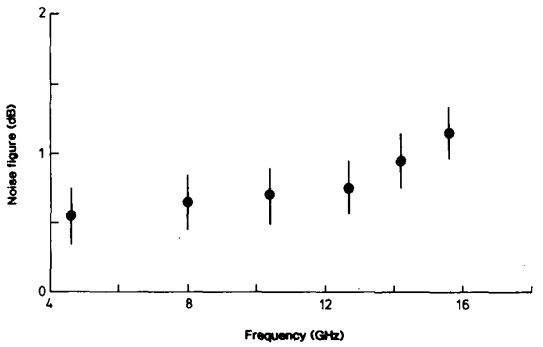

Fig. 7. Noise figure as a function of frequency for a HEMT with a 0.25 × 125 μm gate. Error bars (±0.2 dB are included for each measurement).

est fits correspond to an rms deviation of only ~0.045 dB.

There is no apparent relationship between the final value of the objective function and $|\Gamma_{opt}|$ except for cases where $|\Gamma_{opt}|$ comes up against the constraint. In Fig. 6, results are shown for several devices for which, as a function of $I(ds)$, $|\Gamma_{opt}|$ moves from inside the field of data points to values approaching the upper constraint. The noise figures are seen to vary smoothly right out to the highest values of $|\Gamma_{opt}|$. (The variation of the results for RPH10_3G for low currents is within the observed scatter for high $|\Gamma_{opt}|$.)

The extensive tests carried out on the initial prototype system at 4.78 GHz show it is capable of very repeatable results. The broadband system developed from it produces the same results at 4.78 GHz and similar repeatability at all frequencies. Fig. 7 shows noise figure results at several frequencies for a HEMT. This device, developed at the Division of Radiophysics' laboratory, has a gate with dimensions of 0.25 × 125 μm, and mushroom cross-section to lower gate resistance.

VI. Accuracy

The ultimate precision that can be achieved depends on the accuracy of the calibration of the various instruments used and on the internal consistency of the total measuring system. The latter contributes an uncertainty of about ±0.05 dB as indicated in the results section while the major sources of error are due to calibration.

The sources of error that have been identified are:

calibration of the noise source
calibration of the noise figure meter
uncertainty in the input loss
uncertainty in the output probe loss
possible noise from the p-i-n diode.

TABLE I
NOISE SOURCE CALIBRATION AT 4.78 GHz

Nominal Atten dB	Measured Atten dB	Mean Temp Change Off-On K	Measured ENR dB	Mean ENR dB
20	20.37	57.1	13.32	
16	15.94	157.3	13.29	13.30
13	13.06	304.6	13.28	

TABLE II
NOISE PARAMETER ERRORS (rms)

	Measurement	Calibration	Total
Error in noise figure	0.05	0.19	0.20
Error in $\|\Gamma\|$	0.02	0.006	0.021
Error in phase of Γ	2.0	1.0	2.2
Error in r_n/Z_0	0.04	—	0.04

The ENR (excess noise ratio) for the noise source is specified as having a worst-case uncertainty of 0.3 dB and an rms uncertainty of 0.09 dB. An accurate laboratory radiometer was used to check the noise source calibration against a Maury Microwave MT 7119A cold load. The noise source was attenuated in turn by 13, 16, and 20 dB pads, to keep the output within the linear range of the detector. The attenuators were calibrated using the hp 8510B automatic network analyzer for which the uncertainty specification is <0.05 dB. The resultant ENR for the noise source plus an SMA plug/jack adapter is shown in Table I. The mean ENR was determined to be 13.30 $\pm$ 0.05 dB compared with the nominal value of 13.12 dB. The same set of tests carried out at 12.7 GHz gave an ENR of 14.50 $\pm$ 0.12 dB, again in close agreement with the nominal value of 14.60 dB.

The hp 8970A automatic noise figure meter contributes an instrumentation uncertainty of 0.1 dB in noise figure measurement. It also has an instrumentation uncertainty of 0.2 dB in gain which for the typical gains encountered represents a small fractional uncertainty and makes little contribution to the noise figure errors.

The long-term stability of the input-loss calibration is very good (rms variation over a 112-day period of 0.035 dB). The accuracy of this calibration depends on the hp 8510B automatic network analyzer, and on the quality of the terminations used. Independent checks on the input loss measured directly, without the input probe, confirm the accuracy of the method used. The error in input loss has been estimated to be less than 0.1 dB for our configuration. The output probe loss uncertainty of ~ 0.05 dB makes a negligible contribution to the error budget since it appears only in the output correction.

The possibility of noise being contributed by the p-i-n diode was checked using the radiometer configuration that was employed to measure the noise source ENR. It was found that any departure of the input noise from noise room temperature with the noise source in its off state was less than 1.7% over the range of biases used.

Errors due to calibration and specification uncertainty have the effect of adding to or subtracting from the fitted result, but do not affect the nature of the fit as do random fluctuations in the measurements of the data points. The combined effect of these errors amounts to an rms uncertainty of ± 0.19 dB, which, when combined with the 0.05 dB due to measurements, results in a total rms error of ± 0.2 dB. Table II lists the expected errors for the four noise parameters.

VII. DISCUSSION

In this system, the insertion loss of the probe and the loss associated with the 10 dB coupler, the input line and bias T, combine to limit the magnitude of the reflection that can be presented to the DUT. Because of this, the optimum impedance point for FETs at ~ 5 GHz is usually outside the range of attainable source impedances. In spite of this, the repeatability and quality of the fits give confidence in the results, as do results like those illustrated in Fig. 6. In recent trials, in which large numbers of HEMT's have been measured at 12 GHz, with optimum reflection coefficient generally within the field of measured data points, the excellent stability and reliability have been confirmed.

The range of reflection coefficients presented could be increased by using a directional coupler with lower coupling (e.g., 20 dB), a lower loss bias T, and by substituting a lower loss line for the teflon filled semi-rigid cable presently used.

Increasing the range of the data field might enable the constraints to be relaxed. The constraints were introduced to prevent convergence to nonphysical results ($|\Gamma| > 1$ or $F_{\min} < 1$). Early versions of the algorithm which, in effect, imposed step function constraints had problems with convergence. The manner in which the constraints are now applied results in a smoothly varying error function, and in hundreds of trials, the algorithm currently being used has always converged. Tests have been conducted in which the reflection coefficient has been fixed at a value different from the determined optimum while the remaining parameters have been optimized. It was found that the quality of fit deteriorated rapidly as the reflection coefficient departed from the optimum. This is an indication that the algorithm has arrived at the correct minimum for the data that have been presented, so that any error still present must be in the measurements.

VIII. CONCLUSION

A system has been described that is capable of accurate and reliable on-wafer determination of device noise figure. Changing the bias conditions of a p-i-n diode, together with small frequency changes, enables a range of input impedances to be presented to the DUT. A reliable fitting algorithm enables the four noise parameters to be derived. The system is capable of good throughput, and can cover a broad range of frequencies.

APPENDIX I

A. Input Calibration

The magnitude and phase of the source reflection coefficients at the 16 test points are read directly by the hp8510B automatic network analyzer with the noise source connected to the coupled arm of the coupler. The insertion loss is determined as follows from the measurements of source reflection coefficients with the coupled arm terminated by short and open circuits, and a 50 Ω termination (Γ^s_m, Γ^0_m, Γ^l_m).

Referring to Fig. 3(a) and noting that $S_{12} = S_{21}$ (reciprocal network)

$$a_1 = \frac{1}{S_{12}} b_2 - \frac{S_{22}}{S_{12}} a_2 \tag{A1a}$$

$$b_1 = \frac{S_{11}}{S_{12}} b_2 + \left(S_{12} - \frac{S_{11}S_{22}}{S_{12}} \right) a_2. \tag{A1b}$$

For a short-circuit termination

$$a_2 = -b_2.$$

Substituting in (A1) for a_2 and with a little algebra,

$$\Gamma^s_m = \frac{b_1}{a_1} = \frac{S_{11} - S^2_{12} + S_{11}S_{22}}{1 + S_{22}}. \tag{A2}$$

For an open-circuit termination

$$a_2 = b_2 e^{-j\phi}$$

where ϕ is the offset of the plane of the open circuit, with respect to the short circuit and includes the effect of the open circuit capacitance.

Again, substituting for a_2 leads to

$$\Gamma^0_m = \frac{S_{11} + (S^2_{12} - S_{11}S_{22}) e^{-j\phi}}{1 - S_{22} e^{-j\phi}}. \tag{A3}$$

For a matched termination

$$\Gamma^l_m = S_{11}. \tag{A4}$$

From (A2)

$$\Gamma^s_m(1 + S_{22}) = S_{11} - S^2_{12} + S_{11}S_{22}. \tag{A5}$$

Multiplying (A3) by $e^{j\phi}$, and rearranging, results in

$$\Gamma^0_m(e^{j\phi} - S_{22}) = S_{11}e^{j\phi} + S^2_{12} - S_{11}S_{22}. \tag{A6}$$

Adding (A5) and (A6) and rearranging terms gives

$$S_{22} = \frac{S_{11}(1 + e^{j\phi}) - \Gamma^s_m - \Gamma^0_m e^{j\phi}}{\Gamma^s_m - \Gamma^0_m}. \tag{A7}$$

Rearranging (A5),

$$S_{12} = \sqrt{S_{11} + S_{11}S_{22} - \Gamma^s_m(1 + S_{22})}. \tag{A8}$$

Where the positive sign has been chosen as the solution that gives physically meaningful results. (A4), (A7), and (A8) give the network S-parameters.

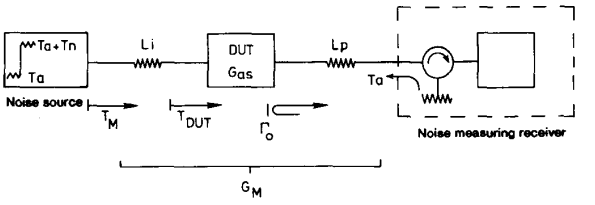

Fig. 8. Simplified schematic diagram of the noise measuring system.

APPENDIX II

A. Noise-Figure Determination

The determination of the device noise figure from the raw measurements is carried out as follows. The simplified schematic of Fig. 8 shows the DUT connected via an input loss (L_i) to a switched noise source, and through an output probe loss (L_P) to an automatic noise-figure meter. The DUT has an output reflection coefficient, Γ_0. As the noise source is switched between its off and on states, the noise-figure meter sees two noise levels which in terms of noise temperature can be written as T_h (noise source on) and T_c (noise source off). The meter determines two quantities from this data, T_M, the measured noise temperature and G_M, the measured gain:

$$G_M = \frac{T_h - T_c}{T_n} \tag{A9}$$

and

$$T_M = \frac{T_c - G_M T_a}{G_M} \tag{A10}$$

where T_n is the input noise step and T_a is the ambient temperature.

The noise incident on the measuring receiver consists of contributions from the noise source, the DUT, the input and output losses, and from the receiver circulator termination reflected in the DUT output. Combining these contributions and taking into account how they are modified by the device's available gain (G_{as}), the losses, and reflection at the device output, results in the following equations for the noise temperatures with the noise source off and on:

$$T_c = L_p(G_{as}(T_{DUT} + T_a)(1 - |\Gamma_0|^2) + |\Gamma_0|^2 T_a) + (1 - L_p)T_a \tag{A11}$$

and

$$T_h = L_p(G_{as}(L_i T_n + T_{DUT} + T_a)(1 - |\Gamma_0|^2) + |\Gamma_0|^2 T_a) + (1 - L_p)T_a \tag{A12}$$

from which

$$G_M = L_i L_p (1 - |\Gamma_0|^2) G_{as} \tag{A13}$$

and

$$T_M = \frac{T_{DUT}}{L_i} + (1 - L_i)\frac{T_a}{L_i} + \frac{L_p|\Gamma_0|^2 T_a + (1 - L_p)T_a}{L_i L_p G_{as}(1 - |\Gamma_0|^2)}. \tag{A14}$$

The required noise temperature and the associated gain are then given by

$$T_{\mathrm{DUT}} = L_i T_M - (1 - L_i) T_a - \frac{(1 - L_p + L_p|\Gamma_0|^2) L_i T_a}{G_M} \tag{A15}$$

and

$$G_{\mathrm{as}} = \frac{G_M}{L_i L_p (1 - |\Gamma_0|^2)}. \tag{A16}$$

The first 2 terms in (A15) correct the measured noise temperature to the input.

Dividing the second term into 2 parts

$$\frac{(1 - L_p) L_i T_a}{G_M} \quad \text{and} \quad \frac{L_i L_p |\Gamma_0|^2 T_a}{G_M},$$

the first part accounts for the noise from the probe loss, while the second part allows for the noise reflected from the device output.

Acknowledgment

The authors thank members of the Solid-State Devices Group at the CSIRO Division of Radiophysics for their support and help with the development of this system. Particular thanks are due to T. Fiocco who performed many of the measurements and contributed to software development and to Dr. W. D. King for his assistance with algorithm convergence.

References

[1] K. R. Gleason, T. M. Reeder, and E. W. Strid, "Precise MMIC parameters yielded by 18 GHz wafer probe," *Microwave Syst. News*, vol. 26, no. 5, pp. 55-65, May 1983.

[2] E. W. Strid, and K. Reed Gleason, "A DC-12 GHz monolithic GaAsFET distributed amplifier," *IEEE Trans. Electron Devices*, vol. ED-29, pp. 1065-1071, July 1982.

[3] V. Adamian, "Test set gauges noise parameters from 6 to 18 GHz," *Microwaves & RF*, vol. 27, pp. 259-261, May 1988.

[4] Cascade Microtech™, NPT 18 Noise Parameter Test Set, Product Literature.

[5] H. Rothe and W. Dahlke, "Theory of noisy fourpoles," *Proc. IRE*, vol. 44, pp. 811-818, June 1956.

[6] IRE Subcommittee 7.9 on Noise, "Representation of noise in linear twoports," *Proc. IRE*, vol. 48, pp. 69-74, Jan. 1960.

[7] R. Q. Lane, "The determination of device noise parameters," *Proc. IEEE*, vol. 57, pp. 1461-1462, Aug. 1969.

[8] R. P. Meys, "A wave approach to the noise properties of linear microwave devices," *IEEE Trans. Microwave Theory Tech.*, vol. MTT-26, pp. 34-37, Jan. 1978.

[9] P. Penfield, "Wave representation of amplifier noise," *IRE Trans. Circuit Theory*, vol. CT-9, pp. 84-86, Mar. 1962.

[10] L. Chusseau, M. Parisot, and N. Jousseaume, "Automatic full noise characterization of microwave GaAs FETs," in *Proc. 17th European Microwave Conf.*, Rome, Italy, Sept. 1987, pp. 628-632.

[11] W. C. Davidon, "Optimally conditioned optimization algorithms without line searches," *Math. Programming*, vol. 9, pp. 1-30, 1975.

[12] D. L. Fenstermacher, "A computer-aided analysis routine including optimization for microwave circuits and their noise," National Radio Astronomy Observatory, Electronics Division Internal Rep. 217, July 1981.

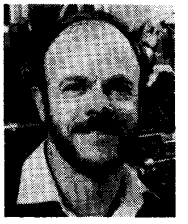

John W. Archer (M'82-SM'83-F'90) was born in Sydney, Australia in 1950. He received the B.Sc., B.E. (Hons I) and Ph.D. degrees from the University of Sydney in 1970, 1972, and 1977, respectively. His Ph.D. led, in 1977, to the development of the first 100 GHz variable-baseline, two-element coherent interferometer for radio astronomy; a joint CSIRO/University of Sydney project.

From 1977 to 1985 he was employed by the National Radio Astronomy Observatory in the United States. The initial two years were spent working on the VLA project where he was responsible for improving the performance of the mm-wave waveguide communications system, as well as designing components for the IF section of the array. The last five years were spent at NRAO's central development laboratory developing state-of-the-art millimeter-wave receiver technology for the Kitt Peak antenna in Arizona. Since 1985 he has been with CSIRO Division of Radiophysics as Leader of the Solid-State Devices Program. He has been responsible for the planning and execution of an $8 million research effort to develop and ultimately commercialize microwave and millimeter-wave GaAs technology in Australia. As well as providing leadership and contributing to a number of significant research achievements, he has been closely associated with efforts to establish commercial manufacturing and marketing of products derived from the Division's research.

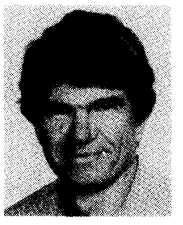

Robert A. Batchelor was born in Sydney, Australia, in 1937. He received the Diploma in Radio Engineering and the B.E. degree in electrical engineering from the University of New South Wales, Australia, in 1959 and 1961, respectively.

From 1955 to 1963 he was employed at Kriesler Australasia Pty. Ltd., doing design work on radio and TV receivers. In 1963 he transferred to the CSIRO Division of Radiophysics. Between 1963 and 1985 he was involved in the design of radio astronomy receivers covering the spectrum from 150 MHz to 115 GHz. During this period he was also engaged in a wide range of radio astronomical observations over the same frequency range. He was a visiting scientist at MIT for 12 months in 1969-1970 and at University of California at Berkeley for four months in 1980-1981, where he was involved in some of the early work on mm-wave SIS mixers. Since 1985 he has been with the Division's Solid-State Devices Program of which he is Deputy Leader. His work in this area has included mask design for low-noise, high-frequency HEMT's, mm-wave Schottky diodes, mm-wave MMIC mixers, and mm-wave power HEMT's. He is responsible for device evaluation. He has also carried out studies of the mm-wave radiation properties of hot steel.